

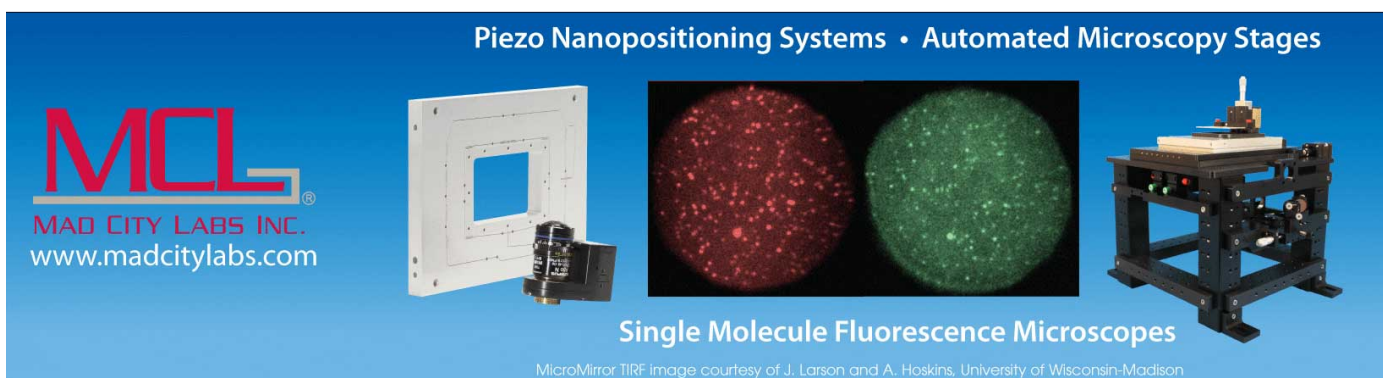
PAPER • OPEN ACCESS

NIR induced modulation of the red emission from erbium ions for selective lanthanide imaging

To cite this article: Stefan Krause *et al* 2018 *Methods Appl. Fluoresc.* **6** 044001

View the [article online](#) for updates and enhancements.

Piezo Nanopositioning Systems • Automated Microscopy Stages



MCL
MAD CITY LABS INC.
www.madcitylabs.com

Single Molecule Fluorescence Microscopes

MicroMirror TIRF Image courtesy of J. Larson and A. Hoskins, University of Wisconsin-Madison

Methods and Applications in Fluorescence



PAPER

NIR induced modulation of the red emission from erbium ions for selective lanthanide imaging

OPEN ACCESS

RECEIVED

25 June 2018

REVISED

24 August 2018

ACCEPTED FOR PUBLICATION

5 September 2018

PUBLISHED

21 September 2018

Original content from this work may be used under the terms of the [Creative Commons Attribution 3.0 licence](#).

Any further distribution of this work must maintain attribution to the author(s) and the title of the work, journal citation and DOI.



Stefan Krause^{1,3} , Mads Koerstz¹ , Riikka Arppe-Tabbara¹, Tero Soukka² and Tom Vosch^{1,3} 

¹ Nano-Science Center/Department of Chemistry, University of Copenhagen, Universitetsparken 5, 2100 Copenhagen, Denmark

² Department of Biotechnology, University of Turku, Medisiina D6, Kiinamylynkatu 10, 20520 Turku, Finland

³ Authors to whom any correspondence should be addressed.

E-mail: stefan.krause@chem.ku.dk and tom@chem.ku.dk

Keywords: lanthanides, photophysics, upconversion, luminescence modulation, imaging

Supplementary material for this article is available [online](#)

Abstract

Upon direct excitation with green light (522 nm), Er³⁺ ion doped nanoparticles feature a number of radiative and non-radiative decay pathways, leading to distinct and sharp emission lines in the visible and near-infrared (NIR) range. Here we apply, in addition to continuous 522 nm irradiation, a modulated NIR irradiation (1143 nm) to actively control and modulate the red emission intensity (around 650 nm). The modulation of red Er³⁺ ion emission at a chosen frequency allows us to reconstruct fluorescence images from the Fourier transform amplitude at this particular frequency. Since only the emission from the Er³⁺ ion is modulated, it allows to selectively recover the lanthanide specific signal, removing any non-modulated auto-fluorescence or background emission resulting from the continuous 522 nm excitation. The modulated emission of specific lanthanides can open up new detection opportunities for selective signal recovery.

Introduction

Lanthanide ion-based emitters have enabled a variety of new methods for optical investigations [1–6]. In upconversion nanoparticle materials, the sequential absorption of multiple photons leads to an anti-Stokes emission signal—referred to as upconversion [7]. Hence, autofluorescence background appearing on the Stokes side of the excitation can be easily suppressed. Due to the small absorption cross-section of the lanthanide-ions, a large number must be combined in a nanoparticle scaffold typically consisting of NaYF₄ in order to create detectable emission [4, 8–12]. Sensitizing these particles with, e.g. ytterbium or organic dyes, further increases the absorption probability [13–16]. The resulting upconversion nanoparticles (UCNPs) have been widely applied in numerous fields of research, such as emissive labels [3, 17, 18], photodetectors [19], multiplexing [20], molecular sensing [21], immunoassays [22], energy transfer [23–26], nanoscopy [27, 28], photodynamic therapy [29], cross-correlation spectroscopy [30], photoacoustic imaging [31] and thermometry [32–35]. The sharp emission and absorption lines of

lanthanide ions are often advantageous and in combination with the long excited state lifetimes, specific excited states can be populated by excitation engineering [36, 37]. Moreover, it has been shown that depletion of specific lanthanide excited states is possible and can be exploited for optical nanoscopy [27, 28, 38].

Here we demonstrate for the first time a combination of direct excitation in the visible range and additional NIR excitation to enhance and modulate the red emission of Er³⁺ UCNPs. We demonstrate the potential of this approach for emission modulation-based imaging by recovering the selective lanthanide signal from environments containing bright organic fluorophores. This selective emission modulation at a constant frequency allows for efficient discrimination of the non-modulated background [39–42].

Results and discussion

Details on the Er³⁺ UCNPs synthesis and size characterization can be found in the supporting information and figure S1 which are available online at [stacks](#).

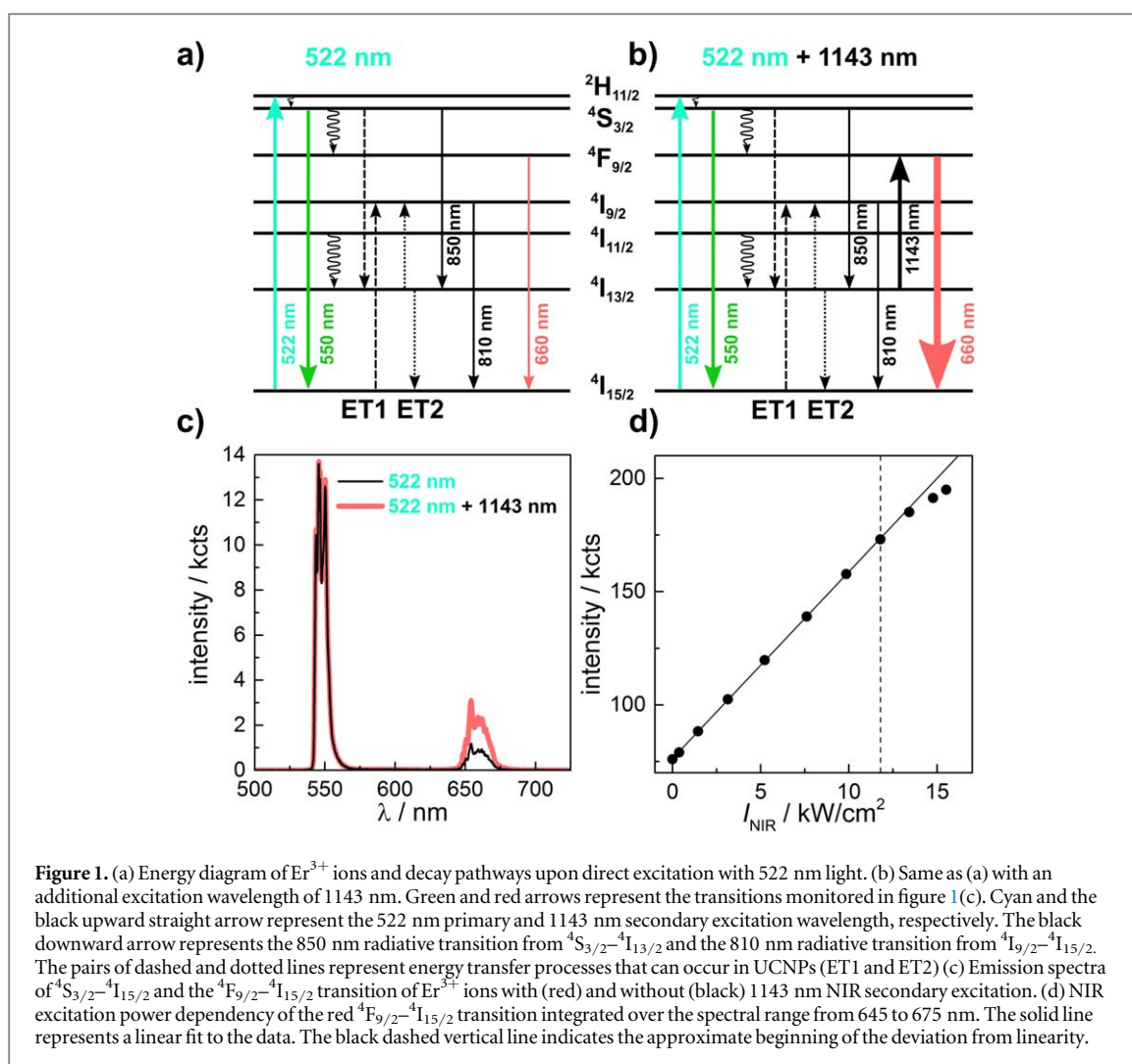
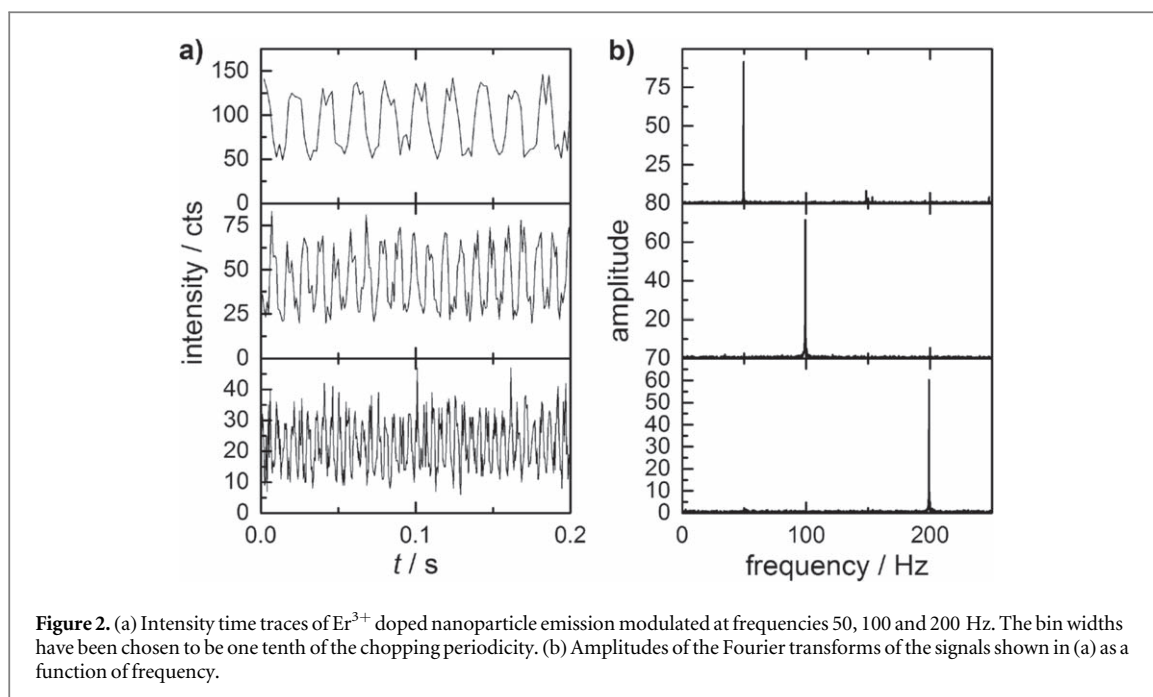


Figure 1. (a) Energy diagram of Er^{3+} ions and decay pathways upon direct excitation with 522 nm light. (b) Same as (a) with an additional excitation wavelength of 1143 nm. Green and red arrows represent the transitions monitored in figure 1(c). Cyan and the black upward straight arrow represent the 522 nm primary and 1143 nm secondary excitation wavelength, respectively. The black downward arrow represents the 850 nm radiative transition from ${}^4\text{S}_{3/2}$ – ${}^4\text{I}_{13/2}$ and the 810 nm radiative transition from ${}^4\text{I}_{9/2}$ – ${}^4\text{I}_{15/2}$. The pairs of dashed and dotted lines represent energy transfer processes that can occur in UCNP (ET1 and ET2) (c) Emission spectra of ${}^4\text{S}_{3/2}$ – ${}^4\text{I}_{15/2}$ and the ${}^4\text{F}_{9/2}$ – ${}^4\text{I}_{15/2}$ transition of Er^{3+} ions with (red) and without (black) 1143 nm NIR secondary excitation. (d) NIR excitation power dependency of the red ${}^4\text{F}_{9/2}$ – ${}^4\text{I}_{15/2}$ transition integrated over the spectral range from 645 to 675 nm. The solid line represents a linear fit to the data. The black dashed vertical line indicates the approximate beginning of the deviation from linearity.

iop.org/MAF/6/044001/mmedia. Figure 1(a) shows the electronic energy diagram of the Er^{3+} ions and the decay pathways that occur upon direct excitation with 522 nm light [43, 44]. The 522 nm laser excites Er^{3+} from the ground state to the ${}^2\text{H}_{11/2}$ state from which the Er^{3+} ions undergo non-radiative transitions to the subsequent energy levels ${}^4\text{S}_{3/2}$ and ${}^4\text{F}_{9/2}$. Besides non-radiative transitions, two emission lines appear on the Stokes side in the visible range at about 550 nm (${}^4\text{S}_{3/2}$ – ${}^4\text{I}_{15/2}$) and 660 nm (${}^4\text{F}_{9/2}$ – ${}^4\text{I}_{15/2}$) [43]. Additional emission lines, such as the NIR emission around 810 nm (${}^4\text{I}_{9/2}$ – ${}^4\text{I}_{15/2}$), 850 nm (${}^4\text{S}_{3/2}$ – ${}^4\text{I}_{13/2}$), 980 nm (${}^4\text{I}_{11/2}$ – ${}^4\text{I}_{15/2}$) and 1530 nm (${}^4\text{I}_{13/2}$ – ${}^4\text{I}_{15/2}$), should also be present [43, 44]. The ${}^4\text{S}_{3/2}$ – ${}^4\text{I}_{13/2}$ transition is of particular importance for populating the ${}^4\text{I}_{13/2}$ state which we will use to modulate the red emission. In order to increase and, hence, modulate the red emission of the ${}^4\text{F}_{9/2}$ – ${}^4\text{I}_{15/2}$ transition, we have chosen a secondary NIR wavelength of 1143 nm that can optically pump the Er^{3+} ions back from the ${}^4\text{I}_{13/2}$ to the ${}^4\text{F}_{9/2}$ excited state (See figure 1(b)). In accordance with the electronic diagram proposed by Anderson *et al* and Würth *et al* this repopulation of ${}^4\text{F}_{9/2}$ from ${}^4\text{I}_{13/2}$ should not have an effect on the 850 nm emission (${}^4\text{S}_{3/2}$ – ${}^4\text{I}_{13/2}$) [43, 44]. The 810 nm emission

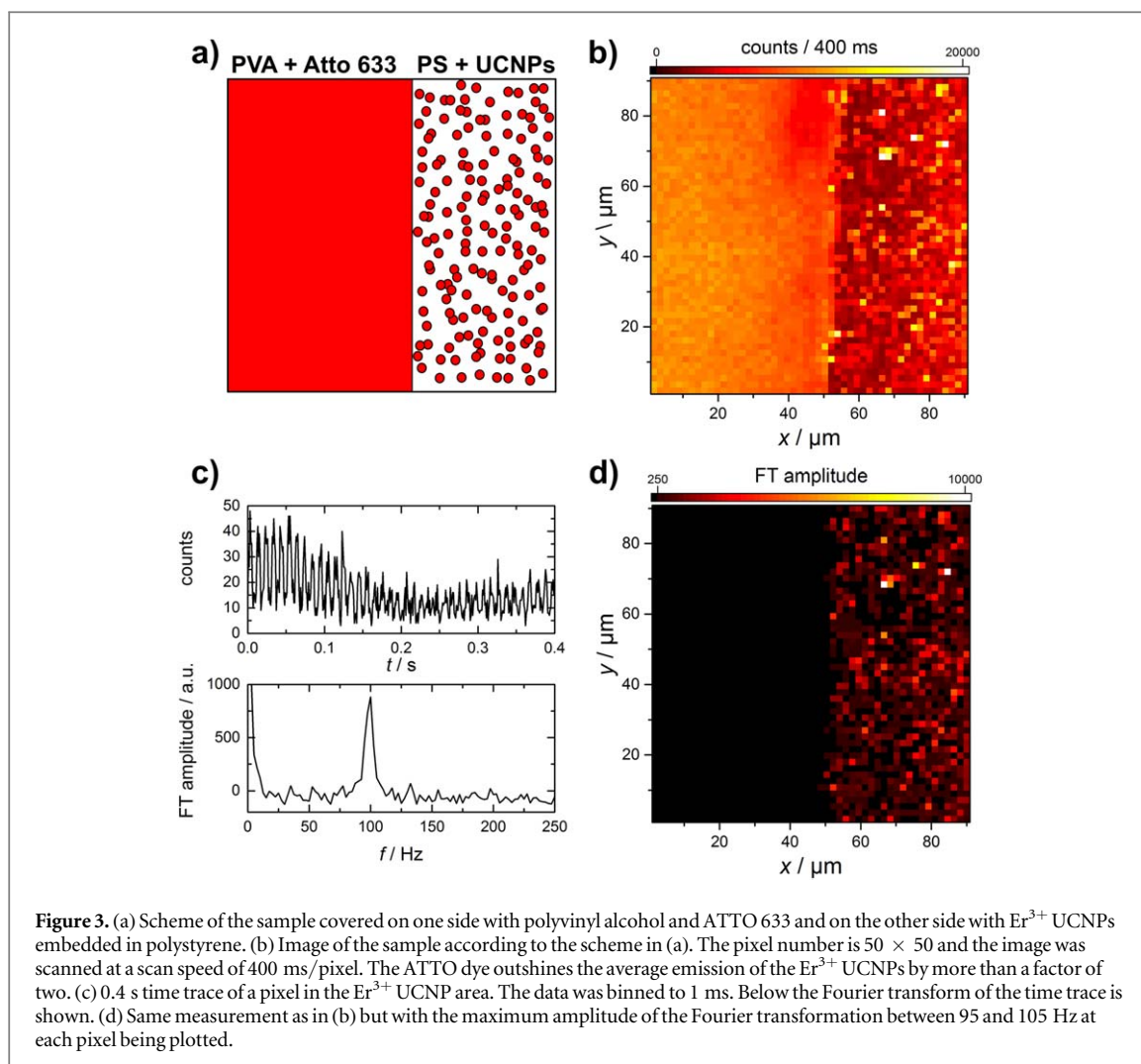
(proposed to originate from energy transfer ET1 of ${}^4\text{S}_{3/2}$ – ${}^4\text{I}_{13/2}$ and ${}^4\text{I}_{15/2}$ – ${}^4\text{I}_{9/2}$ and energy transfer ET2 of ${}^4\text{I}_{13/2}$ – ${}^4\text{I}_{9/2}$ and ${}^4\text{I}_{13/2}$ – ${}^4\text{I}_{15/2}$ in figure 1(a)) [43, 44] might be affected if ET2 and the depopulation of ${}^4\text{I}_{13/2}$ contributes significantly to the 810 nm emission. We measured the 810 nm and 850 nm emission as can be seen in figure S2. The intensity of the 850 nm and 810 nm emission remains unchanged upon NIR modulation which indicates that ET2 does not significantly contribute to the 810 nm emission or is not affected by NIR modulation. Besides emission on the Stokes side, the 522 nm excitation also generates emission on the anti-Stokes side (see figure S3), however this is not of interest for this paper. In order to check the efficiency by which the Er^{3+} UCNP can be pumped back from ${}^4\text{I}_{13/2}$ to ${}^4\text{F}_{9/2}$, we recorded spectra with and without the additional 1143 nm light (See figure 1(c)) of a sample of Er^{3+} UCNP on a glass coverslip. Figure 1(c) shows that at a secondary NIR excitation intensity of 15 kW cm^{-2} , the emission of the 660 nm transition increases more than twofold, while the spectral shape remains unchanged. The amount of additional 660 nm emission is dependent on the decay time of the ${}^4\text{I}_{13/2}$ state (4.4 ms in D_2O) and the intensity of the 1143 nm laser [44]. The latter



was proven by changing the 1143 nm laser intensity while measuring the 660 nm emission as shown in figure 1(d). The dependency follows a linear trend up to about a NIR laser intensity of 12 kW cm^{-2} . Afterwards, the emission intensity seems to deviate from linearity, which might indicate saturation of the optical pumping. Furthermore, the unchanged green emission intensity in figure 1(c) shows that we observe direct optical pumping and not a multiphoton absorption process. Additional factors like temperature, particle size and composition will also have an effect on the observed emission of the UCNP, but they were not the focus of this investigation [34, 35].

After we demonstrated spectrally that our proof of principle works, we continued with measuring the integrated intensity of the red emission shown in figure 1(c) with a long pass/short pass filter combination (creating a transmission window from 633 nm to 750 nm) on an avalanche photo diode (APD) as a function of time. During the measurements, the 1143 nm laser light was modulated on and off by a chopper wheel with adjustable frequency. The resulting intensity time traces can be seen in figure 2(a) for frequencies of 50, 100 and 200 Hz. The ratio between red emission intensities measured with and without 1143 nm irradiation is similar as in the experiment in figure 1(c). From the time traces, we calculated the Fourier transform which is displayed in figure 2(b). As expected, a clear peak in the Fourier transform spectrum can be seen at the frequency that coincides with the frequency settings of the chopper wheel. Although it is possible to modulate the red emission of the Er^{3+} ions at even higher frequencies, problems might arise when approaching a frequency that is close to the inverse of the transit time from ${}^2\text{H}_{11/2} \rightarrow {}^4\text{I}_{13/2}$ [36, 37, 45].

In order to evaluate the Er^{3+} modulation for selective lanthanide signal recovery and imaging, we prepared a sample which consisted on one side of Er^{3+} UCNP embedded in polystyrene (PS) and on the other side of an organic fluorophore (ATTO 633) embedded in polyvinyl alcohol (PVA). A scheme of the sample is shown in figure 3(a). A piezo scanner was used to raster scan the sample while acquiring single photon macro times (time elapsed since the start of the experiment) for each detected single photon with time-correlated single photon counting hardware. In this example, the sample was excited with the 522 nm primary and the 100 Hz modulated 1143 nm secondary excitation wavelength. The intensity image in the spectral bandpass range (633 nm–750 nm) can be seen in figure 3(b) and shows that the ATTO 633 dye (on the left side) displays a homogeneous and, on average, brighter emission than the Er^{3+} UCNP (on the right side). Since the emission of the ATTO 633 dye is not modulated by the 1143 nm laser, removal of this ‘unwanted’ emission can be achieved by constructing an image of the amplitude of the 100 Hz contribution in the FT spectrum. An example of the intensity time trace and FT spectrum at each pixel (time the scanner moves over one pixel is 0.4 s) is given in figure 3(c). For image reconstruction the maximum FT amplitude in the range from 95 to 105 Hz was determined and plotted. The resulting FT amplitude image can be seen in figure 3(d) and shows that the amplitude of the 100 Hz modulation image recovers selectively only the red emission of the Er^{3+} ions, with complete removal of the ATTO 633 emission. Scan time per pixel and modulation frequency will determine the total time and quality of the FT amplitude image.



Conclusion

We have demonstrated the use of multiple excitation wavelengths for manipulating the $^4\text{F}_{9/2}$ and $^4\text{I}_{13/2}$ excited states in Er^{3+} UCNPs. This allowed us to selectively modulate the amplitude of the red emission from the $^4\text{F}_{9/2}$ excited state. Plotting of the corresponding Fourier transform amplitude of the pixel-wise acquired, modulated time traces allowed for selective lanthanide signal recovery and removal of ‘unwanted’ background emission. Application of more powerful visible and NIR laser systems will allow for expanding the presented approach to wide-field microscopy. This will enable for fast selective lanthanide signal recovery and imaging on the seconds time-scale. Our work shows how active control of excited state populations in lanthanides can open up new imaging and sensing applications for this interesting class of elements.

Acknowledgments

We gratefully acknowledge financial support from the ‘Center for Synthetic Biology’ at Copenhagen University funded by the UNIK research initiative of the

Danish Ministry of Science, Technology and Innovation (Grant 09-065274), bioSYnergy, University of Copenhagen’s Excellence Programme for Interdisciplinary Research, the Villum Foundation (Project number VKR023115), the Carlsberg Foundation (CF14-0388), the Danish Council of Independent Research (Project number DFF-7014-00027).

ORCID iDs

Stefan Krause  <https://orcid.org/0000-0002-7062-8472>

Mads Koerttz  <https://orcid.org/0000-0001-5813-6232>

Tom Vosch  <https://orcid.org/0000-0001-5435-2181>

References

- [1] Selvin P R 2002 Principles and biophysical applications of lanthanide-based probes *Annual Review of Biophysics and Biomolecular Structure* **31** 275–302
- [2] Binnemans K 2009 Lanthanide-based luminescent hybrid materials *Chem. Rev.* **109** 4283–374

- [9] Wang F, Banerjee D, Liu Y, Chen X and Liu X 2010 Upconversion nanoparticles in biological labeling, imaging, and therapy *Analyst* **135** 1839–54
- [10] Haase M and Schäfer H 2011 Upconverting nanoparticles *Angewandte Chemie International Edition* **50** 5808–29
- [11] Carro-Temboury M R, Arppe R, Vosch T and Sørensen T J 2018 An optical authentication system based on imaging of excitation-selected lanthanide luminescence *Science Advances* **4** e1701384
- [12] Hyppänen I, Lahtinen S, Ääritalo T, Mäkelä J, Kankare J and Soukka T 2014 Photon upconversion in a molecular lanthanide complex in anhydrous solution at room temperature *ACS Photonics* **1** 394–7
- [13] Auzel F 2004 Upconversion and anti-stokes processes with f and d ions in solids *Chem. Rev.* **104** 139–74
- [14] Heer S, Kömpe K, Güdel H U and Haase M 2004 Highly efficient multicolour upconversion emission in transparent colloids of lanthanide-doped NaYF₄ nanocrystals *Adv. Mater.* **16** 2102–5
- [15] Gnach A and Bednarkiewicz A 2012 Lanthanide-doped up-converting nanoparticles: merits and challenges *Nano Today* **7** 532–63
- [16] Boyer J-C, Vetrone F, Cuccia L A and Capobianco J A 2006 Synthesis of colloidal upconverting NaYF₄ nanocrystals doped with Er³⁺, Yb³⁺ and Tm³⁺, Yb³⁺ via thermal decomposition of lanthanide trifluoroacetate precursors *J. Am. Chem. Soc.* **128** 7444–5
- [17] Wang G, Peng Q and Li Y 2009 Upconversion luminescence of monodisperse CaF₂: Yb³⁺/Er³⁺ nanocrystals *J. Am. Chem. Soc.* **131** 14200–1
- [18] Wang F and Liu X 2008 Upconversion multicolor fine-tuning: visible to near-infrared emission from lanthanide-doped NaYF₄ nanoparticles *J. Am. Chem. Soc.* **130** 5642–3
- [19] Gargas D J et al 2014 Engineering bright sub-10-nm upconverting nanocrystals for single-molecule imaging *Nat. Nanotechnol.* **9** 300
- [20] Garfield D J, Borys N J, Hamed S M, Torquato N A, Tajon C A, Tian B, Shevitski B, Barnard E S, Suh Y D and Aloni S 2018 Enrichment of molecular antenna triplets amplifies upconverting nanoparticle emission *Nat. Photon.* **12** 402–7
- [21] Yang Y, Zhu Y, Zhou J, Wang F and Qiu J 2017 Integrated strategy for high luminescence intensity of upconversion nanocrystals *ACS Photonics* **4** 1930–6
- [22] Zou W, Visser C, Maduro J A, Pshenichnikov M S and Hummelen J C 2012 Broadband dye-sensitized upconversion of near-infrared light *Nat. Photon.* **6** 560
- [23] Hemmer E, Venkatchalam N, Hyodo H, Hattori A, Ebina Y, Kishimoto H and Soga K 2013 Upconverting and NIR emitting rare earth based nanostructures for NIR-bioimaging *Nanoscale* **5** 11339–61
- [24] Liu Q, Sun Y, Yang T, Feng W, Li C and Li F 2011 Sub-10 nm hexagonal lanthanide-doped NaLuF₄ upconversion nanocrystals for sensitive bioimaging *in vivo* *J. Am. Chem. Soc.* **133** 17122–5
- [25] Kataria M, Yadav K, Haider G, Liao Y M, Liou Y-R, Cai S-Y, Lin H-I, Chen Y H, Paul Inbaraj C R and Bera K P 2018 Transparent, wearable, broadband, and highly sensitive upconversion nanoparticles and graphene-based hybrid photodetectors *ACS Photonics* **5** 2336–47
- [26] Lu Y, Zhao J, Zhang R, Liu Y, Liu D, Goldys E M, Yang X, Xi P, Sunna A and Lu J 2014 Tunable lifetime multiplexing using luminescent nanocrystals *Nat. Photon.* **8** 32
- [27] Zhang P, Rogelj S, Nguyen K and Wheeler D 2006 Design of a highly sensitive and specific nucleotide sensor based on photon upconverting particles *J. Am. Chem. Soc.* **128** 12410–1
- [28] Sirkka N, Lyytikäinen A, Savukoski T and Soukka T 2016 Upconverting nanophosphors as reporters in a highly sensitive heterogeneous immunoassay for cardiac troponin I *Analytica Chimica Acta* **925** 82–7
- [29] Mattsson L, Wegner K D, Hildebrandt N and Soukka T 2015 Upconverting nanoparticle to quantum dot FRET for homogeneous double-nano biosensors *RSC Adv.* **5** 13270–7
- [30] Wang L, Yan R, Huo Z, Wang L, Zeng J, Bao J, Wang X, Peng Q and Li Y 2005 Fluorescence resonant energy transfer biosensor based on upconversion-luminescent nanoparticles *Angewandte Chemie International Edition* **44** 6054–7
- [31] Charbonnière L J and Hildebrandt N 2008 Lanthanide complexes and quantum dots: a bright wedding for resonance energy transfer *European Journal of Inorganic Chemistry* **2008** 3241–51
- [32] Yan C, Dadvand A, Rosei F and Perepichka D F 2010 Near-IR photoresponse in new up-converting CdSe/NaYF₄: Yb, Er nanoheterostructures *J. Am. Chem. Soc.* **132** 8868–9
- [33] Zhan Q, Liu H, Wang B, Wu Q, Pu R, Zhou C, Huang B, Peng X, Ågren H and He S 2017 Achieving high-efficiency emission depletion nanoscopy by employing cross relaxation in upconversion nanoparticles *Nat. Commun.* **8** 1058
- [34] Kolesov R, Reuter R, Xia K, Stöhr R, Zappe A and Wrachtrup J 2011 Super-resolution upconversion microscopy of praseodymium-doped yttrium aluminum garnet nanoparticles *Phys. Rev. B* **84** 153413
- [35] Zhang P, Steelant W, Kumar M and Scholfield M 2007 Versatile photosensitizers for photodynamic therapy at infrared excitation *J. Am. Chem. Soc.* **129** 4526–7
- [36] Lahtinen S, Krause S, Arppe R, Soukka T and Vosch T 2018 Upconversion cross-correlation spectroscopy of a sandwich immunoassay *Chemistry—A European Journal* **24** 9229–33
- [37] Wang D, Wei W, Singh A, He G S, Kannan R, Tan L-S, Chen G, Prasad P N and Xia J 2017 Nonlinear photoacoustic imaging by *in situ* multiphoton upconversion and energy transfer *ACS Photonics* **4** 2699–705
- [38] Cui Y, Xu H, Yue Y, Guo Z, Yu J, Chen Z, Gao J, Yang Y, Qian G and Chen B 2012 A luminescent mixed-lanthanide metal-organic framework thermometer *J. Am. Chem. Soc.* **134** 3979–82
- [39] Fischer L H, Harms G S and Wolfbeis O S 2011 Upconverting nanoparticles for nanoscale thermometry *Angewandte Chemie International Edition* **50** 4546–51
- [40] Ranjan S K, Soni A K and Rai V K 2017 Frequency upconversion and fluorescence intensity ratio method in Yb³⁺-ion-sensitized Gd₂O₃: Er³⁺-Eu³⁺ phosphors for display and temperature sensing *Methods. Appl. Fluoresc.* **5** 035004
- [41] Rodrigues E M, Gállico D A, Mazali I O and Sigoli F A 2017 Temperature probing and emission color tuning by morphology and size control of upconverting β-NaYbO₄: 67Gd³⁺, 30F⁴⁺, Tm³⁺, Ho³⁺ nanoparticles *Methods. Appl. Fluoresc.* **5** 024012
- [42] Gainer C F, Joshua G S, De Silva C R and Romanowski M 2011 Control of green and red upconversion in NaYF₄:Yb³⁺, Er³⁺ nanoparticles by excitation modulation *J. Mater. Chem.* **21** 18530–3
- [43] Dawson P and Romanowski M 2018 Excitation modulation of upconversion nanoparticles for switch-like control of ultraviolet luminescence *J. Am. Chem. Soc.* **140** 5714–18
- [44] Stöhr R J, Kolesov R, Xia K, Reuter R, Meijer J, Logvenov G and Wrachtrup J R 2012 Super-resolution fluorescence quenching microscopy of graphene *ACS Nano* **6** 9175–81
- [45] Mao S, Benninger R K, Yan Y, Petchprayoon C, Jackson D, Easley C J, Piston D W and Marriott G 2008 Optical lock-in detection of FRET using synthetic and genetically encoded optical switches *Biophys. J.* **94** 4515–24
- [46] Marriott G, Mao S, Sakata T, Ran J, Jackson D K, Petchprayoon C, Gomez T J, Warp E, Tulyathan O and Aaron H L 2008 Optical lock-in detection imaging microscopy for contrast-enhanced imaging in living cells *Proc. Natl Acad. Sci.* **105** 17789–94
- [47] Richards C I, Hsiang J-C, Senapati D, Patel S, Yu J, Vosch T and Dickson R M 2009 Optically modulated fluorophores for selective fluorescence signal recovery *J. Am. Chem. Soc.* **131** 4619–21
- [48] Zhu Z, Tian D and Shu X 2018 Auto-phase-locked time-gated luminescence detection for background-free upconversion spectra measurement and true-color biological imaging *Sensors Actuators B* **260** 289–94

- [43] Anderson R B, Smith S J, May P S and Berry M T 2013 Revisiting the NIR-to-visible upconversion mechanism in β -NaYF₄: Yb³⁺, Er³⁺ *The Journal of Physical Chemistry Letters* **5** 36–42
- [44] Würth C, Kaiser M, Wilhelm S, Grauel B, Hirsch T and Resch-Genger U 2017 Excitation power dependent population pathways and absolute quantum yields of upconversion nanoparticles in different solvents *Nanoscale* **9** 4283–94
- [45] Karaveli S, Weinstein A J and Zia R 2013 Direct modulation of lanthanide emission at sub-lifetime scales *Nano Lett.* **13** 2264–9